NANO LETTERS

Letter

pubs.acs.org/NanoLett

Epitaxial Growth of DNA-Assembled Nanoparticle Superlattices on Patterned Substrates

Sondra L. Hellstrom,*[,†] Youngeun Kim,[‡] James S. Fakonas,[†] Andrew J. Senesi,[§] Robert J. Macfarlane,[§] Chad A. Mirkin,[‡,§] and Harry A. Atwater[†]

[†]Kavli Nanoscience Institute, California Institute of Technology, Pasadena, California 91125, United States

[‡]Department of Materials Science and Engineering, Northwestern University, Evanston, Illinois 60208, United States

[§]Department of Chemistry, Northwestern University, Evanston, Illinois 60208, United States

Supporting Information

ABSTRACT: DNA-functionalized nanoparticles, including plasmonic nanoparticles, can be assembled into a wide range of crystalline arrays via synthetically programmable DNA hybridization interactions. Here we demonstrate that such assemblies can be grown epitaxially on lithographically patterned templates, eliminating grain boundaries and enabling fine control over orientation and size of assemblies up to thousands of square micrometers. We also demonstrate that this epitaxial growth allows for orientational control, systematic introduction of strain, and designed defects, which extend the range of structures that can be made using superlattice assembly. Ultimately, this will open the door to integrating self-assembled plasmonic nanoparticle materials into on-chip optical or optoelectronic platforms.

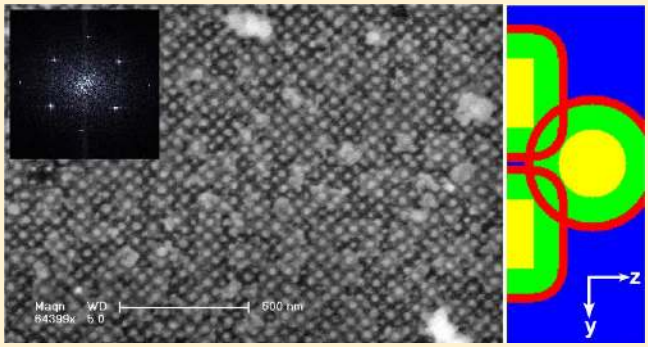

KEYWORDS: *Self-assembly, DNA, nanoparticles, plasmonics, epitaxy*

The assembly of well-ordered, three-dimensional, isotropic, optically active materials has been an important goal in the photonic crystal and metamaterials communities for many years. Many such materials are predicted to have interesting optical properties, including tunable permittivities,[1] complex resonances,[2] and negative refractive indices;[3] these properties are determined mainly by the physical structures of the assemblies, which must be designed and controlled on the nanometer scale. A wide range of techniques exist for constructing these materials,[4,5] including colloidal sedimentation,[6,7] Langmuir−Blodgett trough assembly,[8] drying-based,[9] depletion-based,[10] and matrix-filling[11] strategies. Unfortunately, such techniques lack independent control over the shape, size, and composition of the plasmonic components and the lattice structure. Moreover, the densities of defects are generally high, and the crystal orientations or lattice parameters cannot be easily or widely controlled.

Plasmonic nanoparticles have been assembled a variety of different ways using DNA-based approaches.[12] Indeed, DNA and anisotropically functionalized particles have been used to create clusters that have been described as "small plasmonic molecules".[13−18] DNA origami has also been used to form scaffolds upon which nanoparticles can organize.[19−23] Solutions of these materials have little long-range order, and individual structures are difficult to measure.[24] Nonetheless these materials have been found to exhibit interesting optical properties, including Fano-like resonances[25] and giant circular dichroism.[23] Alternatively, DNA and densely loaded, isotropically functionalized particles have been used to make superlattices with exquisite control over crystal symmetry and lattice parameters.[26−29] Spherical nanoparticles functionalized in this way are referred to as spherical nucleic acids (SNAs)[30] and act as "programmable atom equivalents (PAEs),"[31,32] in which the nanoparticles take the place of atoms, and oligonucleotides take the place of chemical bonds. By adjusting different components of PAEs, hundreds of different crystal structures with both static[29] and dynamic[33,34] tunability have already been made, and a series of design rules has been established to explain and predict solution-phase crystal stability.[29]

Typical PAE superlattices have grain sizes of a few hundred nanometers up to 1−2 μm and form polycrystalline aggregates with uncontrollable edges, sizes, and orientations. To construct and probe a useful optical material, a single crystal on the order of tens of micrometers or larger must be fabricated, with a controllable orientation relative to a substrate and to other optical components. Polycrystalline body-centered cubic (bcc) (100) and (110) thin films have already been grown on

Received: September 9, 2013
Revised: November 6, 2013
Published: November 8, 2013

   dx.doi.org/10.1021/nl4033654 | *Nano Lett.* 2013, 13, 6084−6090

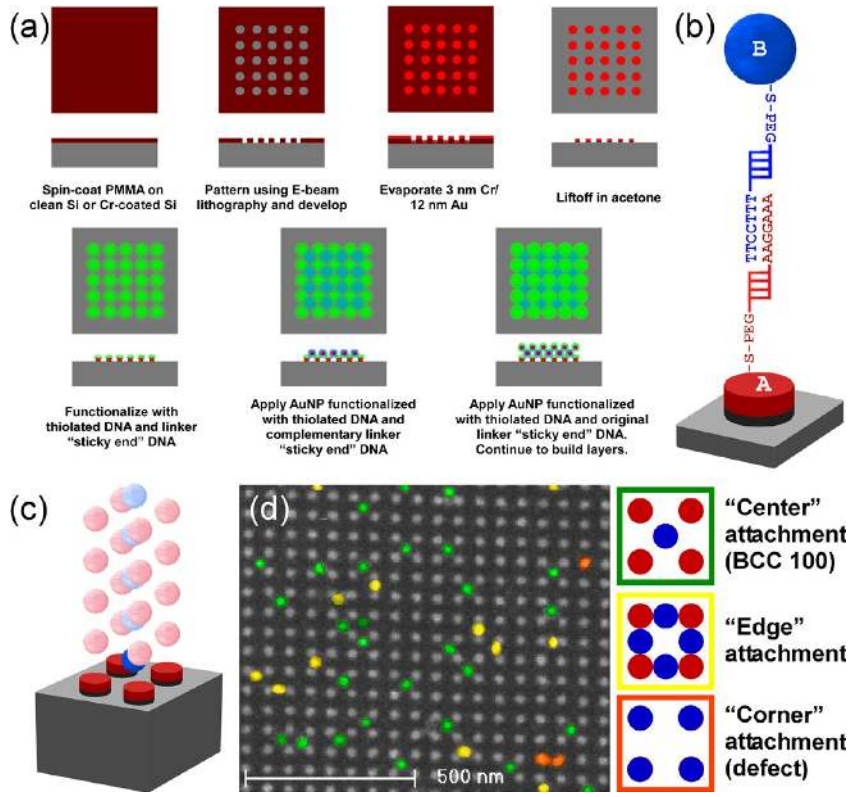

Figure 1. (a) Template fabrication process. (b) Schematic illustrating the DNA binding scheme between template and nanoparticles or between nanoparticles of opposite types (not to scale). (c) Schematic of an ideal bcc (100) crystal epitaxially grown on a surface. Gold surfaces functionalized with DNA containing A-type single stranded ends are shown in red, and gold surfaces with complementary B-type single stranded ends are shown in blue. Full color illustrates the portion discussed in this work. For clarity, the DNA itself is not included. (d) Submonolayer growth on a bcc (100) template, imaged via SEM, with nanoparticles in false color. Submonolayer growth is shown to better illustrate three types of binding modes: center-bound nanoparticles are colored green, edge-bound nanoparticles are colored yellow, and probable corner-bound nanoparticles are colored orange. The associated schematic illustrates these corner, edge, and center-bound particles. In the schematic, template sites presenting A-type sticky ends are shown in red, and deposited particles presenting B-type sticky ends are shown in blue.

unpatterned DNA-modified substrates,[35] opening the door to the formation of crystals with a fixed location and orientation. Although thin-film assemblies grown in this manner with appropriate annealing display a uniaxial texture (preferential orientation normal to the substrate), they remain polycrystalline with domain sizes similar to those of crystals in solution.

Epitaxial growth, that is, the use of a crystalline substrate to control order and orientation in a growing crystal, is typically a very effective method of transferring large-scale order to materials that would otherwise display amorphous or polycrystalline material growth mechanisms.[36] Nonetheless, prepatterned surfaces have only been used in a limited capacity to direct assembly of DNA-modified nanoparticles.[37,38] In this work, in analogy to methods in conventional thin film growth, we have developed a technique to epitaxially grow thin film PAE single crystal superlattices. Electron-beam lithography was used to pattern gold features on silicon; after DNA functionalization, the resulting substrate was roughly equivalent to the first layer of a PAE crystal. We subsequently used this as a template for solution-phase homoepitaxy. Adlayer growth on single-domain 100 μm^2 templates was examined with regards to defect formation, lattice mismatch, and the role of the templated crystal plane on superlattice orientation. We demonstrated control over crystal size, orientation, and location on a substrate, and we also exerted control over defect density and type. This technique will ultimately enable sophisticated optical measurements, assist elucidation of optical structure–property relationships, and potentially extend the range of properties which these materials can exhibit.

Epitaxial growth of bcc superlattices was effected in a manner similar to that used for preparing polycrystalline thin films of PAEs (see Supporting Information),[35] but instead of using an amorphous gold substrate, a nanofabricated one resembling a superlattice crystal plane was employed. Specifically, a template was designed and fabricated using conventional electron-beam lithography in poly(methylmethacrylate) (PMMA; Figure 1a). After exposure and development, 3 nm Ti or Cr and 12 nm Au were sequentially deposited, and the PMMA was lifted off. The fabricated template was then functionalized with 3′-propylthiol-modified DNA, and oligonucleotide linkers with seven base long "sticky ends" were introduced to enable hybridization to PAEs. In this work, we used PAEs with a 30 nm diameter Au core designed to assemble into a bcc crystal with a 62 nm lattice parameter, and we focused on the formation and structure of the first superlattice monolayer. We left our templates exposed to PAE in solution for a full 24 h, to promote the formation of a thermodynamically favorable crystal state.[39]

Lattices with a bcc crystal structure are ideal for use in surface-supported stepwise crystal growth, because they are composed of two complementary distinct types (A and B) of PAE (Figure 1b–c). The bcc crystal is grown by exposing the surface alternately to A-type and B-type nanoparticles, suppressing crystal nucleation in solution. Since the nanoparticles exposed to the surface interact with one another

dx.doi.org/10.1021/nl4033654 | Nano Lett. 2013, 13, 6084–6090

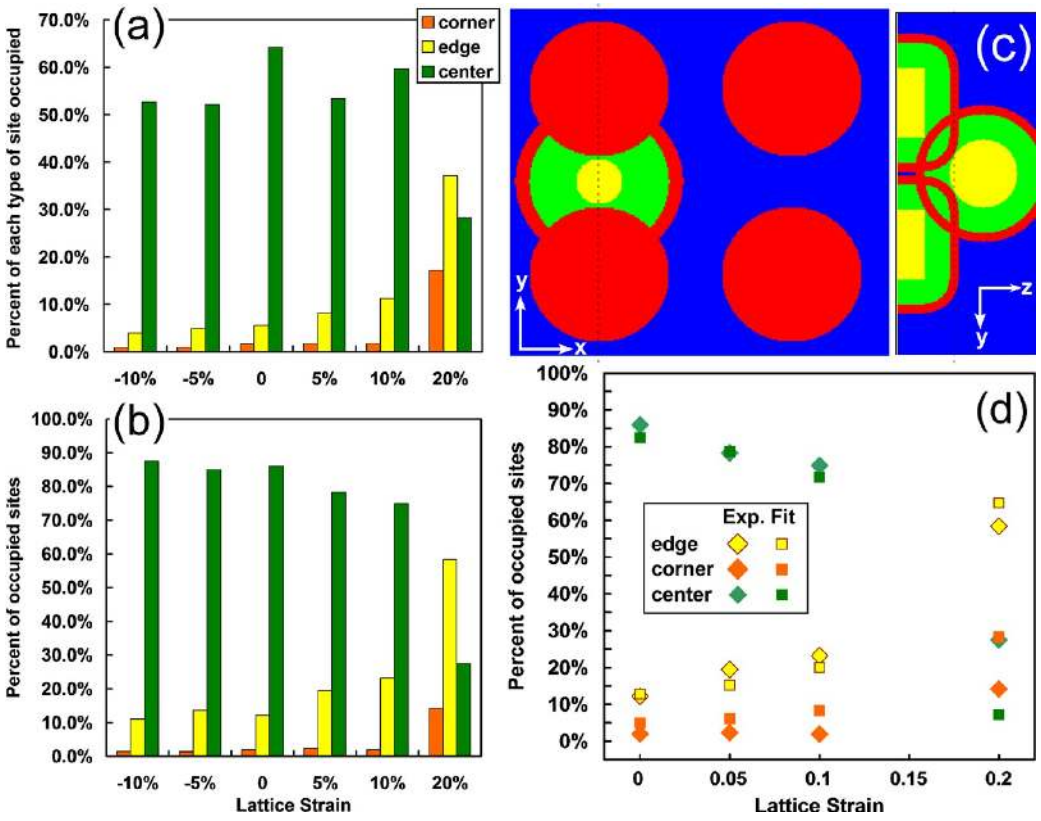

Figure 2. (a) Percent of the specified type of each site occupied by particles, as a function of lattice strain. Note that a particle bound to a given site typically blocks binding to adjacent sites of different types. (b) Percent of the total number of occupied sites that are occupied in the specified manner as a function of lattice strain, illustrating the relative prevalence of each type of binding in a monolayer of particles. (c) *x*- and *z*-plane slices of a simulation used to calculate the degree of DNA hybridization between particles in different configurations (an edge-bound particle is demonstrated in these images). Dashed lines in each scheme illustrate the location of the plane represented in the orthogonal image. Blue space represents buffer, green space represents DNA linker, yellow space represents gold, and red space represents that occupied by a single-stranded DNA sticky end. The amount of DNA hybridization is taken to be proportional to the volume occupied by intersecting red shells. (d) Estimated probabilities of site occupancy fit to (1), with fit parameter $\varepsilon = -2.8$ meV (0.064 kcal/mol) per hybridized sticky end. Qualitative agreement—and the prediction of which site is thermodynamically favorable—is very good.

primarily by steric hindrance and electrostatic repulsion, the attachment of the first adlayer of nanoparticles to the epitaxial substrate is best understood as a process of site-specific adsorption with no driving force for clustering or island growth.

We first studied the adsorption of a monolayer of PAEs on templates designed to be equivalent to a bcc (100) plane. For a submonolayer film, we observed three largely distinct adsorption patterns, corresponding to PAE attachment to either one (corner-bound), two (edge-bound), or four (center-bound) DNA-functionalized lithographic features (Figure 1d). This behavior is most easily observed for submonolayer films but also holds true for full monolayer structures. Since the patterned features on the surface are the equivalents of A-type particles in a bcc lattice, center-bound attachment of PAEs corresponds to the continuation of the lattice. Therefore, in this context edge-bound or corner-bound PAEs constitute defects in the growing crystal. Notably, in contrast to other reports,[40] for substrates composed of Cr films or of Si with native oxide we only rarely found evidence of nonspecific binding of nanoparticles to the substrate surface, even without additional surface functionalization.

For well-ordered lattice-matched monolayer (100) films, vacancies remained the most common kind of defect (Figure 2a). This could have a number of causes, but we believe that two in particular dominate. First, thiol modification of gold surfaces is known to be very dependent on experimental conditions,[41] and we found that the history of the substrate surface prior to modification (type of cleaning and storage) had a strong impact on particle coverage during monolayer growth. This implies that high-density functionalization of the gold template with DNA is important for growing well-ordered monolayers and that variations in oligonucleotide density on the template can lead to vacancies. Second, there is a window of crystallization, temperatures below which nanoparticles cannot diffuse on the substrate surface to promote order, and above which nanoparticle desorption substantially decreases particle coverage.

DNA hybridization occurring at the template surface places a PAE in a lower-energy state compared to a free nanoparticle in solution. The energy benefit to attachment in a given configuration can be calculated using a variant of the "complementary contact model" established in previous work.[29] This model states that the stability of a given arrangement of particles is proportional to the amount of contact between complementary sticky ends on adjacent objects, that is, that the degree of hybridization can be calculated geometrically. In this work we assume that the number of DNA sticky ends that hybridize in a multiparticle system is proportional to the overlapping volume of space between those that contain interpenetrating complementary

dx.doi.org/10.1021/nl4033654 | *Nano Lett.* 2013, 13, 6084−6090

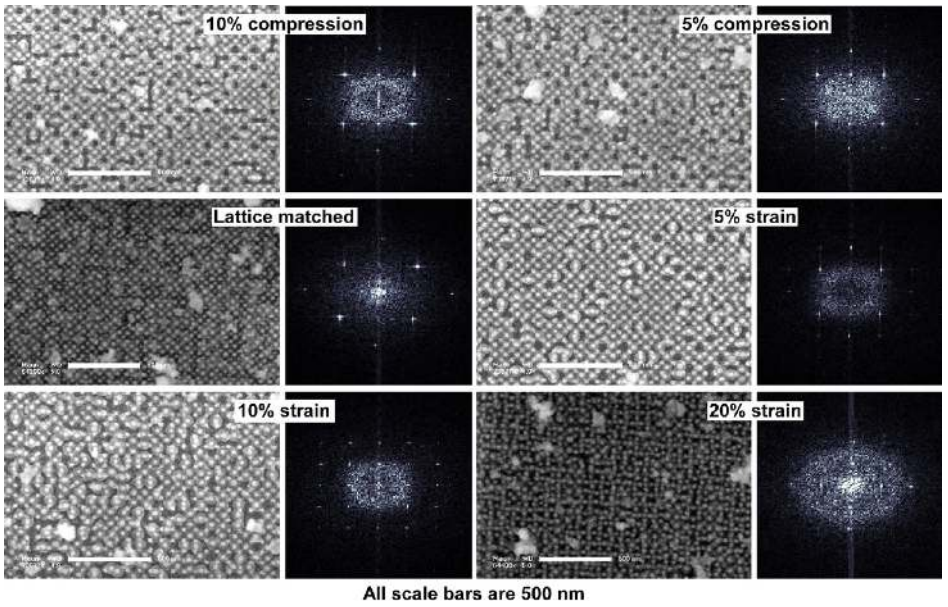

Figure 3. SEM images of monolayer bcc (100) crystals grown on epitaxial templates with −10%, −5%, +5%, +10%, and +20% strain, respectively, as indicated, and two-dimensional fast Fourier transforms of the images, center point removed and cropped to feature lower frequencies. The amorphous matter in the SEM images is left over silica from a sol−gel embedding process required to stabilize the superlattices for drying and imaging with SEM.

sticky ends (for simplicity, the density s of hybridized sticky ends is assumed to be constant in this volume).

Every gold object (yellow) in a functionalized system is modeled as having a halo of sticky ends (red) surrounding it at a distance corresponding to the approximate length of the DNA linker (green) (Figure 2c). We assume that volumes containing DNA are penetrable and volumes containing metal or silicon are not. Then, for a particle in a given configuration, the reduction in energy compared to a free particle is $\Delta E = \varepsilon s V$, where ε is the energy gained by forming a single DNA duplex between two sticky ends and V is the overlapping sticky end volume. Arguably the simplest method of comparing this estimate of the energies of different sites with our experimental observations in Figure 2a−b is with a Boltzmann distribution function. Here, this means that the relative probability of finding a center-bound particle compared to an edge- or corner-bound particle is:

$$p_{\text{center}} = \frac{e^{-\varepsilon s V_{\text{center}}/k_B T}}{\sum_{V=\text{corner,edge,center}} e^{-\varepsilon s V/k_B T}} \quad (1)$$

We calculated overlap volumes for different configurations numerically based on geometry and fit the results to experimental probabilities using eq 1 with ε as a fit parameter (Figure 2d). T and s can be estimated from experimental conditions (here, we use 7.6×10^{-3} sticky ends·nm^{-3}, or approximately 300 sticky ends per 30 nm diameter Au particle, a 4 nm halo,[42] and a temperature of 296 K). Qualitatively, the results match well; in particular, the dominant particle attachment site for a given geometry is always readily predictable. Quantitatively, our fit $\varepsilon = -2.8$ meV per hybridized sticky end is quite small compared with measurements of free DNA hybridization in solution.[43−45] This may be an indication that steric hindrance and electrostatic repulsion substantially counterbalance DNA hybridization in this system or that there are significant sources of disorder other than temperature.

Experimentally, with crystallization at 23 °C, 98% of the particles on our best single lattice-matched 100 μm^2 template were center-bound, clearly demonstrating the viability of large-scale crystal growth using this technique. However, after counting over 5000 attached particles across different substrates, we found that on average 86% of the particles attached to a lattice-matched bcc (100) surface were center-bound (Figure 2b), 12% were edge-bound, and about 2% were corner-bound. We hypothesize that the best method to improve this fraction of center-bound states is to increase the overlap volume of a particle in that state relative to an edge-bound state, by adjusting the geometry of the template. Alternatively, given that for the lattice-matched case the center-bound state is already the one with the greatest overlap volume, a greater percentage of center-bound states could be achieved by increasing ε, or decreasing the crystallization temperature, to the extent possible without inducing kinetic crystallization. In this regard, a process of slow cooling may be helpful in allowing the crystal to most easily settle into its thermodynamically favored state.

To test the flexibility of PAE thin films assembled on lithographically patterned substrates, we investigated growth of the originally designed lattice with a lattice parameter of 62 nm on lithographic features of variable distances (57 nm, 59 nm, 65 nm, 68 nm, and 76 nm) (Figure 3). The amorphous matter in the SEM images is leftover silica from a sol−gel embedding process required to stabilize the superlattices for drying and imaging with SEM.[46]

The most notable defects in the compressed lattices were vacancies. In contrast, strained lattices showed a tendency toward increasing numbers of edge-bound nanoparticles. Up to 10% strain, the first crystal layer grew pseudomorphically with the lattice. However, in the 20% strain case, so many nanoparticles became edge-bound that chains of edge-bound particles became the dominant growth mode. This transition is predictable using calculations of overlap volume (Figure 2d). Around 20% strain, the adlayer began to resemble, were the

dx.doi.org/10.1021/nl4033654 | Nano Lett. 2013, 13, 6084−6090

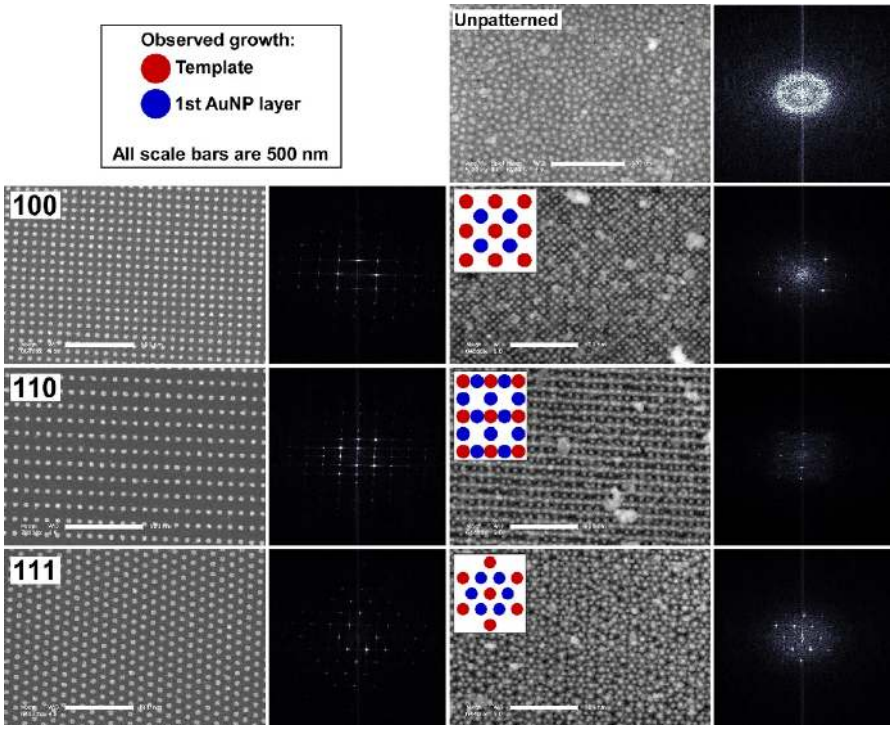

Figure 4. Nanoparticle monolayers attached to bcc (100), (110), and (111) epitaxial templates. From left to right, the images show the templates, a two-dimensional FFT of the template image, the adlayer grown on top of the template, and a two-dimensional FFT of the final image. All FFTs, which were provided to illustrate the degree of order in the films, have their center points removed and are cropped to emphasize lower frequencies. Schematics illustrate the dominant observed growth pattern of PAEs on the templates, with the template in red and the adlayer particles in blue. The amorphous matter in the SEM images is leftover silica from a sol–gel embedding process required to stabilize the superlattices for drying and imaging with SEM.

crystal continued further into three dimensions, a layer consistent with a uniaxially strained bcc (110) lattice—or a bcc (100) lattice with an $a/\sqrt{2}$ lattice parameter and every other center atom missing—rather than a biaxially strained bcc (100). While this result has promise for enabling growth of crystals that cannot be formed in solution or on unpatterned surfaces, the real bulk crystal structure obtained by growth of additional layers on these substrates has yet to be determined.

Using lithographically patterned features allows predictable and programmable control of PAE attachment onto substrates. To test this control, we studied PAE attachment onto templates representing different crystal orientations. Figure 4 shows results of nanoparticle monolayers grown on templates designed to reproduce lattice-matched bcc (100), bcc (110), and bcc (111) crystal planes, compared with a monolayer grown on an unpatterned surface shown as reference. Note that, while the real bcc (110) crystal plane contains both A-type and B-type particles, the template must be fabricated missing the B-type particle, since the surface has only been functionalized with one type of DNA.

In all orientations, a certain defect density notwithstanding, the monolayer adopted a single-domain crystalline structure unique to the patterned surface. This is visible in the two-dimensional fast Fourier transforms of the SEM images, which illustrate that the real crystals maintain the predesigned lattice parameters to a high degree. The nanoparticles attached to all of the templates were physically located in the *x*- and *y*-directions (parallel to the substrate surface), in the locations corresponding to the next layer of particles in bulk three-dimensional bcc (100), (110), and (111) crystals, which makes further growth in these orientations promising.

It is important to note that, while technically speaking the atoms in a bcc lattice are indistinguishable, in the case of the bcc (110) template, half of the nanoparticles in the grown adlayer had the opposite DNA functionalization relative to those in the predicted bulk structure. While the bulk bcc (100) crystal is naturally organized as a layer of A-type particles followed by a layer of B-type particles, this is not the case for bulk bcc (110). Each layer of particles in a bulk bcc (110) crystal contains a mixed composition of A- and B-type particles, one of which is unavailable when only one monolayer is grown. The atoms omitted from the templated crystal plane were not filled in by the grown monolayer, presumably because they were blocked by the silicon substrate. In the case of an unpatterned substrate surface, bulk bcc (110) structures were obtained after multilayer growth and annealing enabled them to relax into their thermodynamically most favorable state. Further experiments with multilayer growth and annealing will tell whether or not such reorganization occurs on epitaxial substrates as well. It is very interesting, though, that even with 50% incorrect functionalization, and without annealing, the particles nevertheless adopted in *x* and *y* the exact symmetry suggested by the (110) template.

A related effect was observed in the bcc (111) system. The bulk bcc (111) crystal is, like the bcc (100), organized as a layer of A-type particles followed by a layer of B-type particles. However, each layer has a comparatively low particle density, which means that substantial potential binding area remains available to particles in solution after a layer is complete. We observed binding of B-type particles to template sites as was consistent with (111) bulk growth, but in addition binding of B-type particles to template sites where A- or B-type particles

dx.doi.org/10.1021/nl4033654 | *Nano Lett.* 2013, 13, 6084–6090

would normally bind at the same x and y but at somewhat different z. This occurred because, at the time of growth, there were no other particles present to block the attachment of the B-type particles to the template. Again, multilayer growth and annealing may reorganize the structure into a true three-dimensional bcc (111) bulk crystal, or alternatively a new three-dimensional strained crystal might be formed. In either case, as with the bcc (110), it is interesting that even with this additional binding the particles adopt in x and y the exact symmetry suggested by the bcc (111) template.

While (100) and (110) orientations can be grown on planar DNA-functionalized substrates through judicious choice of DNA interconnects, higher energy facets such as the (111) orientation are not thermodynamically accessible. Patterning the substrate to appear like (111) seems to force growth consistent with this orientation, albeit with the caveats mentioned above and higher defect density than the other two orientations. This observation suggests that superlattices with novel symmetries not observed in bulk superlattice formation, for example chiral or quasicrystals, may be possible as thin-film superlattices on templated substrates.

In conclusion, we studied epitaxial growth of PAE superlattices and have vastly extended grain sizes in PAE thin films to thousands of square micrometers, limited only by the size of the lithographic template. Further, on this scale we maintained orientation and crystal size control over PAE thin films, which was not possible when crystals were assembled in solution or on unpatterned surfaces. For example, we were able to fabricate strained lattices and higher surface energy orientations by carefully controlling the lattice mismatch and type of lithographically defined template. In addition, we even preprogrammed defects at specific points within the superlattices. We anticipate that this process could be extended to other particle sizes, lattice parameters, and crystal symmetries.

Importantly, this marriage of top-down and bottom-up assembly techniques utilizes the programmability afforded by DNA and the precision and alignment control afforded via lithography to compensate for each techniques' respective drawbacks. We envision that the combination of the two methodologies will have a major impact in both assembling crystal structures not achievable via conventional DNA-programmed assembly or lithography alone, such as lattices with tetragonal or more complex unit cells, with lattice constants larger or smaller than can be currently achieved, and via heteroepitaxial growth involving, for example, different particle shapes or compositions. As a result, we envision that this technique will allow for previously unattainable levels of control over the plasmonic, optical, magnetic, catalytic, or other emergent properties that arise as a result of assembling nanoparticle superlattices.

■ ASSOCIATED CONTENT

Supporting Information

Details of experimental methods, diagrams of bcc lattices, and additional images. This material is available free of charge via the Internet at http://pubs.acs.org.

■ AUTHOR INFORMATION

Corresponding Author

*E-mail: shells@caltech.edu. Address: 1200 E. California Blvd., Pasadena, California, 91125, United States. Tel.: 626-395-3983.

Present Address

A.J.S.: X-ray Science Division, Argonne National Lab, Argonne, Illinois 60439, United States.

Notes

The authors declare no competing financial interest.

■ ACKNOWLEDGMENTS

S.L.H. thanks the Caltech KNI staff for training and equipment expertise; Tiffany Kimoto and Jennifer Blankenship for excellent support; and Dr. Matt Sheldon for technical expertise. H.A.A. and C.A.M. are grateful for funding through the Bioprogrammable One-, Two-, and Three-Dimensional Materials no. FA9550-11-1-0275 MURI. C.A.M. also acknowledges support from the AFOSR (FA9550-12-1-0280) and the DOE (611-8289300-60024682-01) through the NU Non-Equilibrium Research Center. Use of the Advanced Photon Source at Argonne National Laboratory was supported by the U.S. Department of Energy, Office of Science, Office of Basic Energy Sciences, under Contract No. DE-AC02-06CH11357.

■ REFERENCES

(1) Ciattoni, A.; Marinelli, A.; Rizza, C.; Palange, E. |ε|-Near-Zero Materials in the Near-Infrared. *Appl. Phys. B: Laser Opt.* **2013**, *110*, 23−36.

(2) Fan, J. A.; Wu, C.; Bao, J.; Bardhan, R.; Halas, N. J.; Manoharan, V.; Nordlander, P.; Shvets, G.; Capasso, F. Self-Assembled Plasmonic Nanoparticle Clusters. *Science* **2010**, *328*, 1135−1138.

(3) Rockstuhl, C.; Lederer, F.; Etrich, C.; Pertsch, T.; Scharf, T. Design of an Artificial Three-Dimensional Composite Metamaterial with Magnetic Resonances in the Visible Range of the Electromagnetic Spectrum. *Phys. Rev. Lett.* **2007**, *99*, 017401.

(4) Yao, J.; Le, A.-P.; Gray, S. K.; Moore, J. S.; Rogers, J. A.; Nuzzo, R. G. Functional Nanostructured Plasmonic Materials. *Adv. Mater.* **2010**, *22*, 1102−1110.

(5) Hur, K.; Francescanto, Y.; Giannini, V.; Maier, S. A.; Hennig, R. G.; Wiesner, H. Three-Dimensionally Isotropic Negative Refractive Index Materials from Block Copolymer Self-Assembled Chiral Gyroid Networks. *Angew. Chem., Int. Ed.* **2011**, *50*, 11985−11989.

(6) Tao, A. R.; Ceperley, D. P.; Sinsermsuksakul, P.; Neureuther, A. R.; Yang, P. Self-Organized Silver Nanoparticles for Three-Dimensional Plasmonic Crystals. *Nano Lett.* **2008**, *8*, 4033−4038.

(7) Lu, Y.; Yin, Y.; Li, Z.-Y.; Xia, Y. Synthesis and Self-Assembly of Au@SiO_2 Core-Shell Colloids. *Nano Lett.* **2002**, *2*, 785−788.

(8) Tao, A.; Sinsermsuksakul, P.; Yang, P. Tunable Plasmonic Lattices of Silver Nanocrystals. *Nat. Nanotechnol.* **2007**, *2*, 435−440.

(9) Talapin, D. V.; Shevchenko, E. V.; Bodnarchuk, M. I.; Ye, X.; Chen, J.; Murray, C. B. Quasicrystalline Order in Self-Assembled Binary Nanoparticle Superlattices. *Nature* **2009**, *461*, 964−967.

(10) Henzie, J.; Grünwald, M.; Widmer-Cooper, A.; Geissler, P.; Yang, P. Self-Assembly of Uniform Polyhedral Silver Nanocrystals into Densest Packings and Exotic Superlattices. *Nat. Mater.* **2012**, *11*, 131−137.

(11) Vignolini, S.; Yufa, N. A.; Cunha, P. S.; Guldin, S.; Rushkin, I.; Stefik, M.; Hur, K.; Wiesner, U.; Baumberg, J. J.; Steiner, U. A 3D Optical Metamaterial Made by Self-Assembly. *Adv. Mater.* **2012**, *24*, OP23−OP27.

(12) Tan, S. J.; Campolongo, M. J.; Luo, D.; Cheng, W. Building Plasmonic Nanostructures with DNA. *Nat. Nanotechnol.* **2011**, *6*, 268−276.

(13) Alivisatos, A. P.; Johnsson, K. P.; Peng, X.; Wilson, T. E.; Loweth, C. J.; Bruchez, M. P., Jr.; Schultz, P. G. Organization of "Nanocrystal Molecules" using DNA. *Nature* **1996**, *382*, 609−611.

(14) Loweth, C. J.; Caldwell, W. B.; Peng, X.; Alivisatos, A. P.; Schultz, P. G. DNA-Based Assembly of Gold Nanocrystals. *Angew. Chem., Int. Ed.* **1999**, *38*, 1808−1812.

(15) Mastroianni, A. J.; Claridge, S. A.; Alivisatos, A. P. Pyramidal and Chiral Groupings of Gold Nanocrystals Assembled Using DNA Scaffolds. *J. Am. Chem. Soc.* **2009**, *131*, 8455−8459.
(16) Maye, M. M.; Nykypanchuk, D.; Cuisinier, M.; van der Lelie, D.; Gang, O. Stepwise Surface Encoding for High-Throughput Assembly of Nanoclusters. *Nat. Mater.* **2009**, *8*, 388−391.
(17) Xu, X.; Rosi, N. L.; Wang, Y.; Huo, F.; Mirkin, C. A. Asymmetric Functionalization of Gold Nanoparticles with Oligonucleotides. *J. Am. Chem. Soc.* **2006**, *128*, 9286−9287.
(18) Pal, S.; Sharma, J.; Yan, H.; Liu, Y. Stable Silver Nanoparticle−DNA Conjugates for Directed Self-Assembly of Core-Satellite Silver−Gold Nanoclusters. *Chem. Commun.* **2009**, 6059−6061.
(19) Pal, S.; Deng, Z.; Ding, B.; Yan, H.; Liu, Y. DNA-Origami-Directed Self-Assembly of Discrete Silver-Nanoparticle Architectures. *Angew. Chem., Int. Ed.* **2010**, *49*, 2700−2704.
(20) Ding, B.; Deng, Z.; Yan, H.; Cabrini, S.; Zuckermann, R. N.; Bokor, J. Gold Nanoparticle Self-Similar Chain Structure Organized by DNA Origami. *J. Am. Chem. Soc.* **2010**, *132*, 3248−3249.
(21) Aldaye, F. A.; Sleiman, H. F. Dynamic DNA Templates for Discrete Gold Nanoparticle Assemblies: Control of Geometry, Modularity, Write/Erase and Structural Switching. *J. Am. Chem. Soc.* **2007**, *129*, 4130−4131.
(22) Aldaye, F. A.; Sleiman, H. F. Sequential Self-Assembly of a DNA Hexagon as a Template for the Organization of Gold Nanoparticles. *Angew. Chem., Int. Ed.* **2006**, *45*, 2204−2209.
(23) Kuzyk, A.; Schreiber, R.; Fan, Z.; Pardatscher, G.; Roller, E.-M.; Högele, A.; Simmel, F. C.; Govorov, A. O.; Liedl, T. DNA-Based Self-Assembly of Chiral Plasmonic Nanostructures with Tailored Optical Response. *Nature* **2012**, *483*, 311−314.
(24) Sebba, D. S.; Mock, J. J.; Smith, D. R.; LaBean, T. H.; Lazarides, A. A. Reconfigurable Core-Satellite Nanoassemblies as Molecularly-Driven Plasmonic Switches. *Nano Lett.* **2008**, *8*, 1803−1808.
(25) Fan, J. A.; He, Y.; Bao, K.; Wu, C.; Bao, J.; Schade, N. B.; Manoharan, V. N.; Schvets, G.; Nordlander, P.; Liu, D. R.; Capasso, F. DNA Enabled Self-Assembly of Plasmonic Nanoclusters. *Nano Lett.* **2011**, *11*, 4859−4864.
(26) Mirkin, C. A.; Letsinger, R. L.; Mucic, R. C.; Storhoff, J. J. A DNA-Based Method for Rationally Assembling Nanoparticles Into Macroscopic Materials. *Nature* **1996**, *382*, 607−609.
(27) Park, S. Y.; Lytton-Jean, A. K. R.; Lee, B.; Weigand, S.; Schatz, G. C.; Mirkin, C. A. DNA-Programmable Nanoparticle Crystallization. *Nature* **2008**, *451*, 553−556.
(28) Nykypanchuk, D.; Maye, M. M.; van der Lelie, D.; Gang, O. DNA-Guided Crystallization of Colloidal Nanoparticles. *Nature* **2008**, *451*, 549−552.
(29) Macfarlane, R. J.; Lee, B.; Jones, M. R.; Harris, N.; Schatz, G. C.; Mirkin, C. A. Nanoparticle Superlattice Engineering with DNA. *Science* **2011**, *334*, 204−208.
(30) Cutler, J. I.; Auyeung, E.; Mirkin, C. A. Spherical Nucleic Acids. *J. Am. Chem. Soc.* **2012**, *134*, 1376−1391.
(31) Macfarlane, R. J.; O'Brien, M. N.; Petrosko, S. H.; Mirkin, C. A. Nucleic Acid-Modified Nanostructures as Programmable Atom Equivalents: Forging a New "Table of Elements". *Angew. Chem., Int. Ed.* **2013**, *52*, 5688−5698.
(32) Zhang, C.; Macfarlane, R. J.; Young, K. L.; Choi, C. H. J.; Hao, L.; Auyeung, E.; Liu, G.; Zhou, X.; Mirkin, C. A. A General Approach to DNA-Programmable Atom Equivalents. *Nat. Mater.* **2013**, *12*, 741−746.
(33) Maye, M. M.; Kumara, M. T.; Nykypanchuk, D.; Sherman, W. B.; Gang, O. Switching Binary States of Nanoparticle Superlattices and Dimer Clusters by DNA Strands. *Nat. Nanotechnol.* **2010**, *5*, 116−120.
(34) Kim, Y.; Macfarlane, R. J.; Mirkin, C. A. Dynamically Interchangeable Nanoparticle Superlattices Through the Use of Nucleic Acid-Based Allosteric Effectors. *J. Am. Chem. Soc.* **2013**, *135*, 10342−10345.
(35) Senesi, A. J.; Eichelsdoerfer, D. J.; Macfarlane, R. J.; Jones, M. R.; Auyeung, E.; Lee, B.; Mirkin, C. A. Stepwise Evolution of DNA-Programmable Nanoparticle Superlattices. *Angew. Chem., Int. Ed.* **2013**, *52*, 6624.
(36) Venables, J. A. *Introduction to Surface and Thin Film Processes*; Cambridge University Press: New York, Nov 6, 2000.
(37) Kershner, R. J.; Bozano, L. D.; Micheel, C. M.; Hung, A. M.; Fornof, A. R.; Cha, J. N.; Rettner, C. T.; Bersani, M.; Frommer, J.; Rothemund, P. W. K.; Wallraff, G. M. Placement and Orientation of Individual DNA Shapes on Lithographically Patterned Surfaces. *Nat. Nanotechnol.* **2009**, *4*, 557−561.
(38) Lalander, C. H.; Zheng, Y.; Dhuey, S.; Cabrini, S.; Bach, U. DNA-Directed Self-Assembly of Gold Nanoparticles onto Nano-patterned Surfaces: Controlled Placement of Individual Nanoparticles into Regular Arrays. *ACS Nano* **2010**, *4*, 6153−6161.
(39) Macfarlane, R. J.; Lee, B.; Hill, H. D.; Senesi, A. J.; Seifert, S.; Mirkin, C. A. Assembly and organization processes in DNA-directed colloidal crystallization. *Proc. Natl. Acad. Sci. U.S.A.* **2009**, *106*, 10493−10498.
(40) Kannan, B.; Kulkarni, R. P.; Majumdar, A. DNA-based Programmed Assembly of Gold Nanoparticles on Lithographic Patterns with Extraordinary Specificity. *Nano Lett.* **2004**, *4*, 1521−1524.
(41) Herne, T. M.; Tarlov, M. J. Characterization of DNA Probes Immobalized on Gold Surfaces. *J. Am. Chem. Soc.* **1997**, *119*, 8916−8920.
(42) Chi, Q.; Wang, G.; Jiang, J. The Persistence Length and Length per Base of Single-Stranded DNA Obtained from Fluorescence Correlation Spectroscopy Measurements Using Mean Field Theory. *Physica A* **2013**, *392*, 1072−1079.
(43) Holbrook, J. A.; Capp, M. W.; Saecker, R. M.; Record, M. T., Jr. Enthalpy and Heat Capacity Changes for Formation of an Oligomeric DNA Duplex: Interpretation in Terms of Coupled Processes of Formation and Association of Single-Stranded Helices. *Biochemistry* **1999**, *38*, 8409−8422.
(44) Mikulecky, P.; Feig, A. L. Heat Capacity Changes Associated with DNA Duplex Formation: Salt- and Sequence-Dependent Effects. *Biochemistry* **2006**, *45*, 604−616.
(45) Biancaniello, P. L.; Kim, A. J.; Crocker, J. C. Colloidal Interactions and Self-Assembly Using DNA Hybridization. *Phys. Rev. Lett.* **2005**, *94*, 058302.
(46) Auyeung, E.; Macfarlane, R. J.; Choi, C. H. J.; Cutler, J. I.; Mirkin, C. A. Transitioning DNA-Engineered Nanoparticle Superlattices from Solution to the Solid State. *Adv. Mater.* **2012**, *24*, 5181−5186.